Synchrotron-based High Resolution Far-infrared Spectroscopy of *trans*-butadiene

Marie-Aline Martin-Drumel[1], Jessica P. Porterfield[2], Manuel Goubet[3], Pierre Asselin[4], Robert Georges[5], Pascale Soulard[4], Matthew Nava[6], P. Bryan Changala[7], Brant Billinghurst[8], Olivier Pirali[1], Michael C. McCarthy[2], and Joshua H. Baraban[9]

[1] *Université Paris-Saclay, CNRS, Institut des Sciences Moléculaires d'Orsay, 91405 Orsay, France*
[2] *Center for Astrophysics, Harvard & Smithsonian, Cambridge, Massachusetts 02138, United States*
[3] *Université Lille, CNRS, UMR 8523-PhLAM-Physique des Lasers, Atomes et Molécules, F-59000 Lille, France*
[4] *Sorbonne Universités, UPMC Univ Paris 06, UMR 8233, MONARIS, F-75005 Paris, France & CNRS, UMR 8233, MONARIS, F-75005 Paris, France*
[5] *Institut de Physique de Rennes, CNRS, UMR 6251, Université de Rennes 1, F-35042 Rennes, France*
[6] *Department of Chemistry, Harvard University, Cambridge, MA 02138, United States*
[7] *JILA, University of Colorado, Boulder, CO 80309, United States*
[8] *Canadian Light Source, University of Saskatchewan, Canada*
[9] *Department of Chemistry, Ben-Gurion University of the Negev Beer-Sheva 8410501, Israel*

Contact corresponding author(s): marie-aline.martin@universite-paris-saclay.fr

The high resolution far-infrared spectrum of *trans*-butadiene has been re-investigated by Fourier-transform spectroscopy at two synchrotron radiation facilities, SOLEIL and the Canadian Light Source, at temperatures ranging from 50 to 340 K. Beyond the well-studied bands, two new fundamental bands lying below 1100 cm^{-1}, ν_{10} and ν_{24}, have been assigned using a combination of cross-correlation (ASAP software) and Loomis-Wood type (LWWa software) diagrams. While the ν_{24} analysis was rather straightforward, ν_{10} exhibits obvious signs of a strong perturbation, presumably owing to interaction with the dark $\nu_9 + \nu_{12}$ state. Effective rotational constants have been derived for both the $v_{10} = 1$ and $v_{24} = 1$ states. Since only one weak, infrared active fundamental band (ν_{23}) of *trans*-butadiene remains to be observed at high resolution in the far-infrared, searches for the elusive *gauche* conformer can now be undertaken with considerably greater confidence in the dense ro-vibrational spectrum of the *trans* form.

1. Introduction

Much attention has surrounded 1,3-butadiene (C_4H_6) because this conjugated diene is an ideal candidate to observe the effects of π-electron delocalization [1, 2], and because it is of central importance in a wide range of chemistry applications, from its archetypal role in the Diels-Alder reaction [3] to industrial rubber production [4]. Characterizing the structural conformers and isomerization dynamics of this diene, however, has proven surprisingly challenging. 1,3-butadiene exists in two stable forms, the more stable planar *trans*, and the long-elusive *gauche*, lying 12 kJ/mol higher in energy [5]. The latter was only conclusively detected in the gas phase recently by several authors of the present work, an effort which also yielded a nearly complete semi-experimental equilibrium structure (r_e^{SE}) from a combination of pure rotational measurements of various isotopic species and high-level quantum chemical calculations [5].

While electron diffraction studies provided insight into the structure of *trans*-butadiene as early as the late 1930's [6, 7], an accurate determination of its equilibrium structure was only achieved in 2006 [1]. This centro-symmetric species possesses no permanent dipole moment, and consequently no pure rotational spectrum. Determination of the ground state constants thus relied on the assignments of rotational transitions in its dense vibrational bands, a challenging feat overcome in 2004 with the high-resolution analysis of three infrared bands — namely ν_{17} (3100 cm^{-1}) [8], ν_{11} (908 cm^{-1}) [9], and ν_{20} (1596 cm^{-1}) [9]. From extensive isotopic investigations, Craig and co-workers [1] soon afterwards derived a full semi-experimental structure from the ground state rotational

constants of eight isotopologues: the normal [9], 1,1-d_2 [10], 2,3-d_2 [9], 1,4-*trans*,*trans*-d_2 [11], 1,4-*cis*,*cis*-d_2 [11], 1,4-*cis*,*trans*-d_2 [11], 1-$^{13}C_1$ [12], and 2,3-$^{13}C_2$ [13] species. With the notable exception of butadiene-1,1-d_2 which is slightly polar and was thus investigated using microwave spectroscopy by Caminati et al. [10], the rotational constants of all other isotopologues were derived from high-resolution ro-vibrational measurements.

trans-butadiene belongs to the C_{2h} point group and possesses 12 IR-active modes, 4 of a_u and 8 of b_u symmetries. Among them, 6 modes lie below 1100 cm^{-1}, *i.e.* in the far-IR domain: ν_{13} (162.42 cm^{-1}, a_u) [14], ν_{24} ($\sim$ 299.1 cm^{-1}, b_u)[15], ν_{12} (524.57 cm^{-1}, a_u) [14], ν_{11} (908.07 cm^{-1}, a_u) [9], ν_{23} ($\sim$ 990.3 cm^{-1}, b_u) [15], and ν_{10} ($\sim$ 1013.8 cm^{-1}, a_u) [15]. Of these, only three — ν_{10}, ν_{23}, and ν_{24} — have not been observed at high resolution prior to this work, and thus their band centers (listed above) are probably accurate to at most a few wavenumbers based on low resolution gas phase investigation [15]. In this article, we report the first ro-vibrational analysis of two of these, ν_{10} (out-of-plane C−H wagging[16]) and ν_{24} (in-plane C=C−C deformation[16]). The spectra were recorded at two synchrotron radiation facilities, SOLEIL and the Canadian Light Source (CLS), during a search for the ro-vibrational spectrum of the *gauche*-butadiene.

2. Methods

2.1. Quantum chemical calculations

Vibrational frequencies and rotational constants were computed by second-order vibrational perturbation theory (VPT2)[17]. The force field constants were obtained using a hybrid approach, wherein a coupled-cluster treatment of electron correlation with singles, doubles, and perturbative triples and the frozen-core approximation [fc-CCSD(T)] was employed with the ANO1 basis set for the harmonic frequencies and the ANO0 basis set for the anharmonic constants[18]. Calculations were performed using the CFOUR suite of electronic structure programs [19]. The expected far-IR spectrum of butadiene from literature experimental values, when available, or these calculations, otherwise, is simulated in Fig 1. Tables S1 and S2 report the calculated band centers and intensities, and the calculated rotational constants, respectively.

A particularly noteworthy result of the VPT2 calculations is the predicted resonance between $v_{10} = 1$ (a_u symmetry) and $v_9 = v_{12} = 1$ (a_u), whose zero-order energies lie less than 1 cm^{-1} apart, around 1034 cm^{-1}, according to the ANO1 harmonic frequencies. Using the GUINEA module of CFOUR with hybrid ANO1/ANO0 constants, the effective Hamiltonian between the $v_{10} = 1$ and $v_9 = v_{12} = 1$ states has been constructed and diagonalized. Once anharmonicity is taken into account, the states are found to be 22 cm^{-1} apart (with $v_{10} = 1$ lower in energy, lying at 1012 cm^{-1} and $v_9 = v_{12} = 1$ lying at 1034 cm^{-1} , see Table S1) with an overall (pure vibrational) coupling matrix element of 0.8 cm^{-1}.

2.2. Butadiene sample preparation

In all of the experiments performed here, 1,3-butadiene was synthesized from thermal decomposition of sulfolene ($C_4H_6SO_2$) at 85–100 °C according to the reversible reaction:

$$C_4H_6SO_2(s) \rightleftharpoons^{\Delta} C_4H_6(g) + SO_2(g). \quad \textbf{(1)}$$

Theoretical calculations of this reaction [20] predict gaseous butadiene is initially produced in the *gauche* form through a *cis* transition state via a retro-Diels-Alder mechanism.

To prevent the reverse Diels-Alder reaction, and to obtain a high purity sample of butadiene, an SO_2 trap consisting of KOH pellets was used:

$$SO_2(g) + KOH(s) \longrightarrow K_2SO_3(s) + H_2O(l), \quad \textbf{(2)}$$

where water released during reaction Eq. (2) was condensed in a cold trap maintained at about 0 °C. Butadiene passes through this trap, but was subsequently collected either by condensation in a vessel cooled with liquid nitrogen or was directly injected into the measurement cell. This purification procedure precludes the obtainment of nonthermal rotamer populations of butadiene (*gauche:trans* ratio) due to numerous collisions with the vessel walls.

2.3. Synchrotron-based FT-IR spectroscopy

The high resolution ro-vibrational spectrum of butadiene has been investigated using three complementary set-ups installed at two synchrotron facilities, SOLEIL and the Canadian Light Source. These set-ups allowed us to probe the sample at three different temperatures, namely 50, 273, and 343 K. In all cases, butadiene spectra were recorded using Fourier-transform spectroscopy (in the far- and mid-IR) using a Bruker IFS125HR spectrometer at its ultimate resolution of about 1×10^{-3} cm^{-1}. When used as the light source, the synchrotron radiation was focused onto the entrance iris of the interferometer. In all cases, the interferometer was continuously evacuated to 10^{-5} mbar to minimize absorption by atmospheric water. Each experiment is described in greater details in the following paragraphs.

2.3.1. Warm cell experiment

A synchrotron-based ro-vibrational spectrum of butadiene was recorded in the 400–1300 cm^{-1} region at the far-IR beamline of the CLS facility [21]. About 40 µbar of sample was injected into a 2-m base-length multipass White-type cell aligned for a 72 m optical path length and maintained at a 343 K (70 °C) temperature [22]. The cell was separated from the interferometer using KBr windows. 280 scans were collected at 0.00096 cm^{-1} resolution (according to Bruker definition) using a 80kHz scanner velocity, a 1.15 mm entrance iris aperture, a KBr beamsplitter, and a Ge:Cu detector installed inside a QMC pulse tube cooled cryostat, and equipped with a KRS5 window.

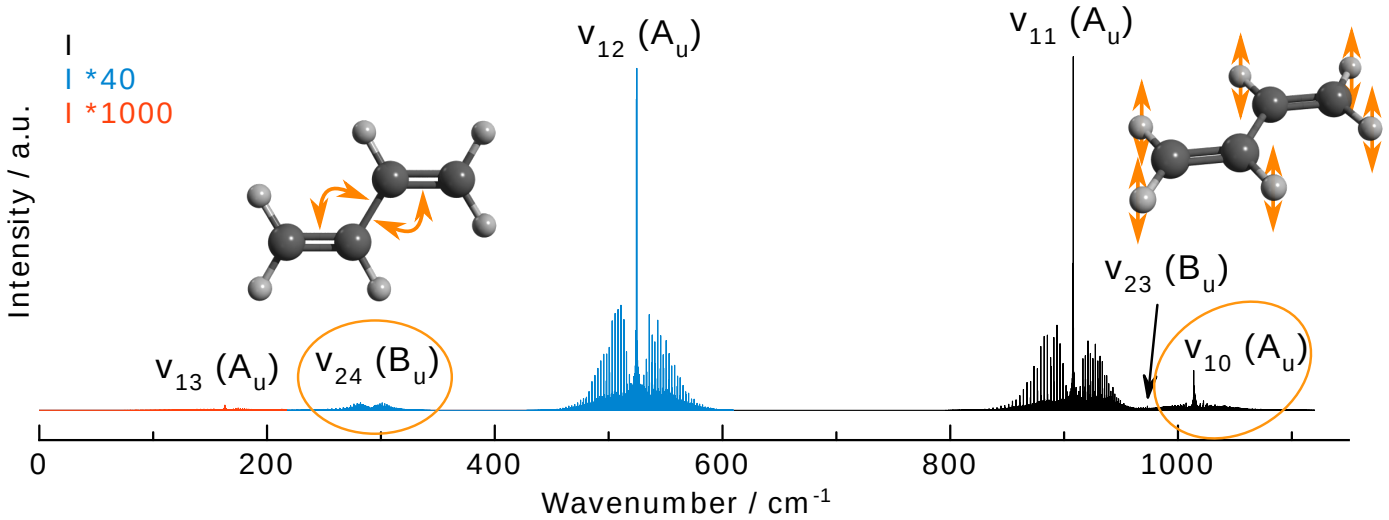


Fig. 1. Simulation of the high resolution (at 0.001 cm^{-1} resolution and assuming a Doppler profile) far-IR spectrum of *trans*-butadiene (fundamental bands only) performed with the PGOPHER software using the experimental band centers and rotational constants when available, or those derived from the quantum chemical calculations (Table S1-S2). Computed intensities are plotted in arbitrary units. For the sake of clarity, the weak bands have been magnified by a factor 40 (ν_{12}, ν_{24}, in blue) or 1000 (ν_{13}, in red). The two new bands investigated in this work (ν_{10} and ν_{24}) have been highlighted in orange and the deformation associated with the two corresponding vibrations is represented by orange arrows on the molecular pictures.

The spectrum was calibrated using residual lines from HDO (around 1200 cm^{-1}), HCN (around 715 cm^{-1}), and CO_2 (around 670 cm^{-1}) whose rest wavenumbers were taken from the HITRAN database [23] and includes experimental data pertinent to this work [24–26]. Residual lines of water, saturated in our experimental spectrum, were not considered in the calibration procedure. From the difference between the calibrated wavenumbers and the reference ones, accuracy of line positions for the entire spectrum should be better than $\pm 2 \times 10^{-4}$ cm^{-1} (Fig. S1). Around 1100 cm^{-1}, where the ν_{10} band of butadiene is predicted to lie, the Doppler full width at half maximum of the lines at 343 K is of about 2×10^{-3} cm^{-1}; thus, a wavenumber accuracy of about a tenth that value appears appropriate.

2.3.2. Room temperature experiment

A synchrotron-based ro-vibrational spectrum of butadiene was recorded in the 50–650 cm^{-1} region at the AILES beamline of the SOLEIL synchrotron facility [27]. A spectrum consisting of 220 co-added interferograms was recorded at a resolution of 0.00102 cm^{-1} (Bruker definition) using a 2.5-m base-length room temperature multipass White-type cell aligned for about 150 m optical path length [28] and filled with 180 µbar of sample. A 2 mm iris, a 6 µm thick mylar-silicon composite beamsplitter, and a liquid-helium Si bolometer were used for the measurements. The cell was isolated from the interferometer by two 50 µm thickness polypropylene windows.

Calibration was performed using residual H_2O and CO_2 lines whose reference wavenumbers were taken from Refs. 29, 30, which in turn allowed line frequencies to be determined to better than $\pm 1 \times 10^{-4}$ cm^{-1} below 500 cm^{-1} and $\pm 2 \times 10^{-4}$ cm^{-1} above 500 cm^{-1} (Fig. S1).

2.3.3. Supersonic-jet experiment

Finally, a spectrum of butadiene in a supersonic jet expansion was recorded in the 850–1050 cm^{-1} region using the Jet-AILES apparatus at SOLEIL[31, 32]. A slit nozzle of 60 mm length and 130 µm width was used to expand the sample seeded in helium buffer gas, with respective flows of 1 and 20 standard liters per minutes (slm), into a large chamber that was continuously evacuated by a set of Roots pumps. The reservoir and chamber pressures were maintained at 260 and 0.8 mbar, respectively, and the chamber was separated from the interferometer and the detection compartment by two KBr windows. The high resolution spectrum is the result of the co-addition of 130 individual scans recorded at 0.00102 cm^{-1} resolution using a globar source, a 1.13 mm iris aperture, a KBr beamsplitter, and photovoltaic MCT detector. A low-pass optical filter was placed in front of the detector thereby limiting the upper wavenumber value of the measurements to 1050 cm^{-1}. Under our experimental conditions, the use of the synchrotron radiation instead of the globar source resulted in a lower signal-to-noise ratio.

Additional spectra were recorded at lower resolution (0.01 cm^{-1}) for different sample to buffer gas ratios (2 slm of butadiene and x slm of He, where $x = 0, 5, 10, 20, 30$) but otherwise identical experimental conditions. Since

accurate rotational constants of the ν_{11} band of *trans*-butadiene were available from prior work[9], simulations of the band profile (using the PGOPHER software [33]) allowed us to infer the rotational temperature of the spectra with different mixing ratios. A temperature of 30 K well reproduced the high resolution Jet-AILES spectrum, while temperatures of 150, 100, 70, 50, and 40 K were estimated to reproduce the lower resolution spectra with 0, 5, 10, 20, and 30 slm of He, respectively (Fig. S2).

In the relatively narrow range covered by the Jet-AILES spectrum, only two bands of *trans*-butadiene, ν_{10} and ν_{11}, are visible, which precludes a conventional frequency calibration using standard molecules. Instead, calibration was performed by comparing strong, isolated lines in both the well-calibrated warm spectrum recorded at CLS with those in this jet spectrum. Several drawbacks to this procedure should be noted: i) the wavenumber accuracy of the CLS transitions is at best 2×10^{-4} cm^{-1} whereas accuracy as low as 1×10^{-4} cm^{-1} should be possible in the cold Jet-AILES spectrum owing to the narrower lines and sparser spectrum that arises at colder rotational temperatures; and ii) because of the temperature difference between the two spectra, lines that are strong in the Jet-AILES spectrum may not be intense in the CLS spectrum, and *vice versa*. To increase our calibration reliability, we have selected as many lines as possible on the Jet-AILES spectrum that correspond to lines having a transmittance higher than 0.2 in the warm CLS spectrum. A conservative wavenumber accuracy of 5×10^{-4} cm^{-1} is expected from this procedure (Fig. S1).

2.4. Analysis procedure

Since several ro-vibrational bands of *trans*-butadiene have previously been assigned at high resolution, it is reasonable to assume that the vibrational ground state is very well-described, even though no pure rotational measurements of the main isotopologue are available. As a consequence, analysis of the newly-recorded bands appears well-suited for the Automated Spectral Analysis Approach (ASAP) developed by C. P. Endres and several of the authors of this paper [34, 35]. Briefly, this procedure facilitates fast analysis of a ro-vibrational band when one of the two vibrational levels involved, the so-called reference state, is well-characterized. The second, or target state is thus the one from which spectroscopic information needs to be extracted. The method exploits the power of the Loomis-Wood approach for ro-vibrational assignments (see, *e.g.*, Refs. 36, 37) and the redundancy of the spectroscopic information in a ro-vibrational band with multiple selection rules (typically P-, Q-, R-branches and asymmetric splitting), *i.e.* when transitions originating from different rotational energy levels of the reference state reach the same rotational energy level of the target state. Since the energy levels of the reference state are well-determined, the error in the predicted ro-vibrational frequencies between the reference and target state are dominated by the error in the prediction of the target state. Since each set of transitions reaches the same rotational level, the frequencies of the sought-after experimental transitions all share the same offset relative to their prediction, with the value of that offset being the error in the predicted energy of the particular target rotational level. Assigning ro-vibrational transitions in such a set thus entails identifying lines lying at the same offset value from the prediction in each portion of the spectrum. ASAP simplifies this step by cross-correlating (multiplying) these portions of the spectrum. For spectra plotted in absorbance, the signal approaches zero between transitions, provided the spectrum is well-resolved. Thus, most frequency points will be multiplied by zero at least once except if a line is always present on each plot. This method allows for significant spectral simplification, as only a few points will stand out from the baseline, and by plotting successive J values in a Loomis-Wood fashion, one can assign series of lines. One consequence of the cross-correlation is that the actual ro-vibrational frequencies are no longer assigned; rather the energy of the sought after target state is directly extracted (predicted energy + assigned offset). Since it is no longer necessary to assign each transition for each selection rule, but only the target energy levels involved in the band, this procedure greatly speeds-up analysis time. The energy levels together with other available data are input to the SPFIT/SPCAT suite of programs[38] to derive the rotational constants and band center of the target state.

The ASAP method has proven extremely helpful in assigning several bands of S_2O, for which the rotational ground state was accurately known from extensive pure rotational investigations [34, 35]. In the present case, however, since no such pure rotational data exists and since the ro-vibrational bands assigned in the literature were recorded at similar or lower resolution compared to the present work, once the target state rotational constants were derived from the ASAP analysis, a conventional assignment of each ro-vibrational transition was also undertaken. To do so, the LWWa software developed by W. Lodyga was used [37].

3. Results and discussion

3.1. Initial fit of the literature data

To obtain ground state constants that are as accurate as possible, we have refitted all of the ro-vibrational data previously published, *i.e.* in the ν_{11} [9], ν_{12} [14], ν_{13} [14], ν_{17} [8], and ν_{20} [9] bands. A Watson S-reduced Hamiltonian in the I^r representation and the Pickett SPFIT program were used. Since $A >> B \sim C$, we have chosen S-reduction although literature data were fitted using the A-reduction. Data from ν_{12} and ν_{13} [14] were weighted according to their experimental uncertainty (0.0002 cm^{-1}), while those in ν_{11} and ν_{20} [9], for which the estimated line accuracy was not stated, were weighted using the standard deviation obtained in the fit reported by the authors (0.0002 and 0.007 cm^{-1}, respectively). In the case of ν_{17}, the authors [8] noted that the expected wavenumber accuracy

on each transition should be 10 times better than the standard deviation of their fit (0.003 cm^{-1}) but perturbations, most likely from a rovibrational dark state, limited the fit convergence. Since in our study no attempt was made toward treating this perturbation, the value of this standard deviation was retained as the line uncertainty. In total, 7015 transitions (6929 different frequencies) are included in our fit with $J'' = 0 - 73$ and $K_a'' = 0 - 18$. All quartic centrifugal distortion (CD) terms were varied in the ground state while those unfitted in the excited states were constrained to the ground state value. By using a 5σ rejection criterion (i.e. transitions were discarded if the observed−calculated frequency was five or more times the postulated uncertainty), 16 lines from Refs. 9, 14 were rejected from the fit. In these instances, it appears that the inability to reproduce the literature data to within the experimental accuracy is due to perturbations rather than misassignments. We have therefore decided to keep these lines in the fit but to reduce their wavenumber accuracy by a factor 10 (see Table S4 for the list of transitions). The reduced standard deviation (unitless) of the combined fit is 1.16, ranging from 0.73 to 1.54 for individual bands. To our knowledge, only ground state combination differences and some individual ro-vibrational bands were fitted together prior to this study. Since a combined effective fit has been performed here, the ground state rotational constants should be quite reliable.

3.2. The ν_{24} vibrational band

The ν_{24} band of *trans*-butadiene (*a*/*b* hybrid) is observed in the room temperature spectrum recorded at SOLEIL (Fig. 2).

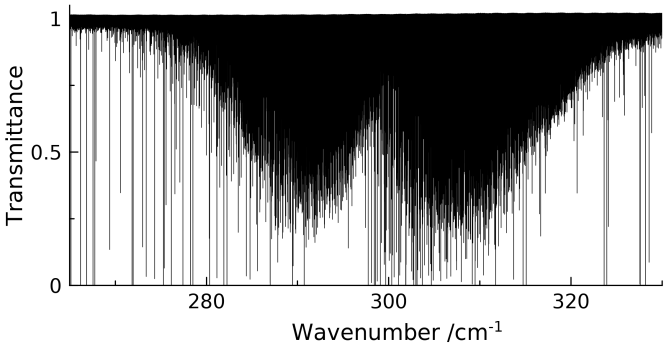


Fig. 2. Overview of the high-resolution spectrum of the ν_{24} band of *trans*-butadiene observed at room temperature. Isolated lines arise from residual water vapor, and most of these are saturated. A portion of the Q-branch is also saturated.

ASAP assignments Using the ground state as the reference state and $v_{24} = 1$ as the target state, ASAP searches were performed. The initial rotational constants for $v_{24} = 1$ were obtained by scaling the VPT2 results by the experimentally-derived versus calculated constants in the ground state (Table S1-S2). The initial frequency for the band center was taken from the low-resolution gas phase assignment of Ref. 15.

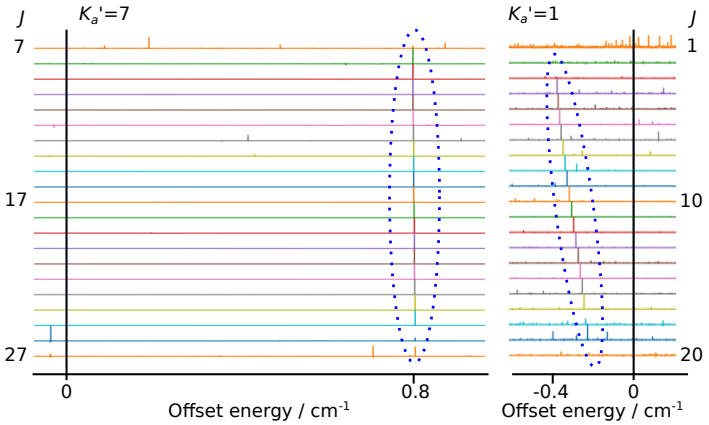


Fig. 3. Initial ASAP views of the ν_{24} band (*left panel*, for one of the two $K_a' = 7$ asymmetric branches) and the ν_{10} band (*right panel* for a $K_a' = 1$ branch). Predicted energies are represented by the black vertical line (0 cm^{-1} offset) and visible series of lines are highlighted in blue.

Because several series of lines are readily identifiable on the ASAP plots (Fig. 3), a preliminary assignment of the band could be performed almost immediately; it consists of 290 energy levels in $v_{24} = 1$ with $J' = 4 - 44$, $K_a' = 4 - 14$, measured to 0.0001 cm^{-1} accuracy. These energy levels were then added to the list of literature assignments, as defined in the previous section, and constants fit using the Pickett software. The resulting parameters are reported in Table 1. Even though we suspected that inclusion of higher-order CD parameters would help to reduce the standard deviation, at this juncture of the analysis the number of fitted parameters was limited because it appeared that the energies derived in the ASAP procedure were not as accurate as expected given our experimental resolution. Ostensibly this situation arises because of residual error in the ground (reference) state energies owing to the absence of extremely accurate pure rotational data. Indeed, after fitting, the ASAP series are still not uniformly aligned, and the distribution of residuals is larger than expected for a spectrum recorded at a resolution of 0.001 cm^{-1}. This may come from the fact that the data defining the ground state has at best an uncertainty twice what we expect from the ν_{24} measurements (0.0002 vs. 0.0001 cm^{-1}). Additionally, some Q-branch lines are saturated, which induces broadening of the ASAP lines. Because it is not possible to omit specific lines in the cross-correlation procedure using the current version of the software, this effect may skew the ASAP plots. For both of these reasons, a subsequent line-by-line assignment of the ν_{24} band has been performed using the LWWa software.

LWWa assignments Using the preliminary constants derived for $v_{24} = 1$, assignments using the LWWa software are straightforward. Comparison of the LWWa diagrams with those from ASAP (Fig. 4) indicates that lines ap-

pear better aligned (i.e. have a smaller dispersion) compared to the former plots. It should be noted, however, that the LWWa software represents a line as a triangle placed at its center frequency, with no consideration for the width of the actual line, while the ASAP plot displays a cross-correlated line profile. Nevertheless, the LWWa plots allow assignment over a wider range of quantum numbers without ambiguity. In total, 2840 transitions with $J' = 4 - 87$ and $K'_a = 2 - 18$ have been assigned with a frequency uncertainty of 0.0001 cm^{-1} using this approach.

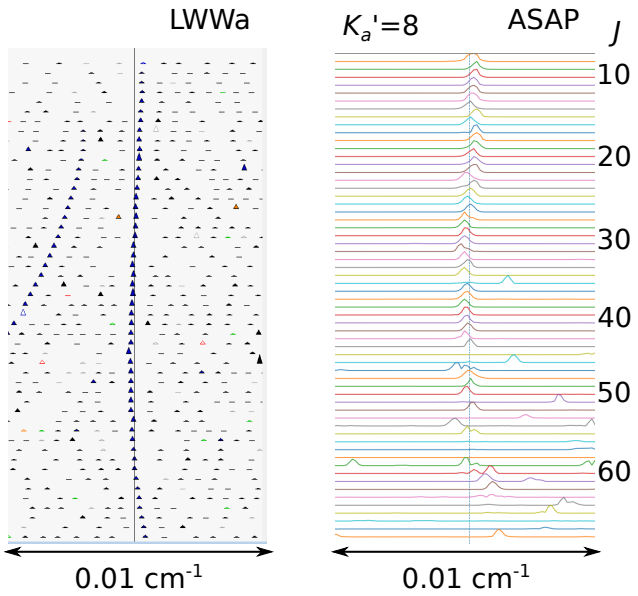


Fig. 4. Initial LWWa view of the ν_{24} band for one of the two $K'_a = 8$ branches in comparison with the corresponding final ASAP plot (i.e., following the initial fit).

3.3. The ν_{10} vibrational band

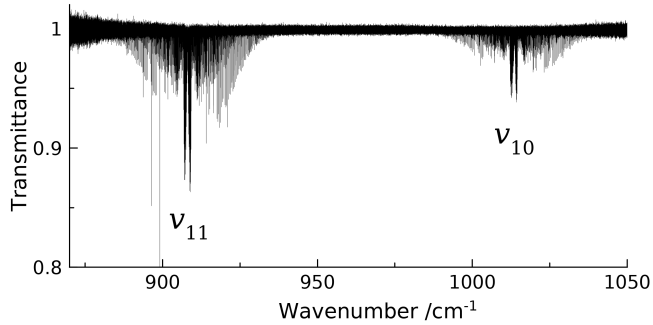


Fig. 5. Overview of the high resolution, rotationally cold spectrum recorded using the Jet-AILES apparatus: both the ν_{10} and ν_{11} bands of *trans*-butadiene are clearly visible.

The *c*-type ν_{10} vibrational band of butadiene was observed both in the cold supersonic jet spectrum recorded at SOLEIL (Fig. 5) and in the warm one recorded at CLS. During the measurements with the supersonic jet, we were also able to observe the effect of rotational cooling on the band profile: from a standard *c*-type band with a sharp Q-branch at moderate temperature, the band evolves to a completely different profile with two Q-branch lobes at low temperature (Fig. 6).

ASAP assignments Following the same procedure as for the ν_{24} band, assignments were first performed using the ASAP software. The ground state was used as the reference state, the initial constants of the target state (here $v_{10} = 1$) were obtained by scaling the VPT2 calculation (Table S2), and the initial frequency of the band center was taken from the low-resolution gas-phase assignment of Ref. 15.

As with the ν_{24} analysis, several series of lines, slightly displaced from the prediction, were readily observed and assigned (Fig. 3): over 100 energy levels in total, with $J' = 1 - 24$ and $K'_a = 0 - 6$. As before, the reduced standard deviation of the fit, assuming a 0.0005 cm^{-1} accuracy for the energy levels, is high ($\sigma = 16$ when fitting a single quartic CD term in addition to the rotational constants and band center; see Table 1). Owing to the limited range of the quantum numbers that are accessible at this temperature, no additional CD terms were varied at this stage of the analysis.

LWWa assignments Using the preliminary set of rotational constants and the LWWa software we were able to assign 927 lines with 682 different frequencies, including 131 lines with $\Delta K_c = \pm 2$, in the Jet-AILES spectrum. These transitions involve $J' = 1 - 29$ and $K'_a = 0 - 7$.

Additionally, 1176 transitions (964 different frequencies) were also assigned in the warm CLS spectrum with $J' = 2 - 49$ and $K'_a = 0 - 7$. More lines, likely involving higher J and K_a values, are present in the warm spectrum, but it was not possible to assign them with confidence using our best model (see the Combined fit section).

3.4. Other bands

In the FIR spectra we recorded, limited sensitivity prevented detection of any combination bands. Searches for ν_{23} (lying around 977 cm^{-1}) were also unsuccessful. This band is expected to be extremely weak (see Fig. 1 and Table S1) and increasing the pressure in hopes of detecting it resulted in full optical saturation of ν_{10} and ν_{11} in the room temperature and warm spectra.

3.5. Combined effective fit

A fit has been performed using the Pickett software for all the literature data and the newly assigned transitions. Energy levels assigned at the ASAP step were not included, nor were the assignments of the ν_{10} band from the warm CLS spectrum (only the cold Jet-AILES data were considered for this band). The best-fit constants and relevant fit parameters for the ν_{10} and ν_{24} bands are summarized in Table 1, while the complete set of constants (all states in the fit) is given in Table S3. For ν_{24}, inclusion of two higher-order (sextic and octic: H_K and L_K) CD terms, not needed for the ground state, are required to reproduce

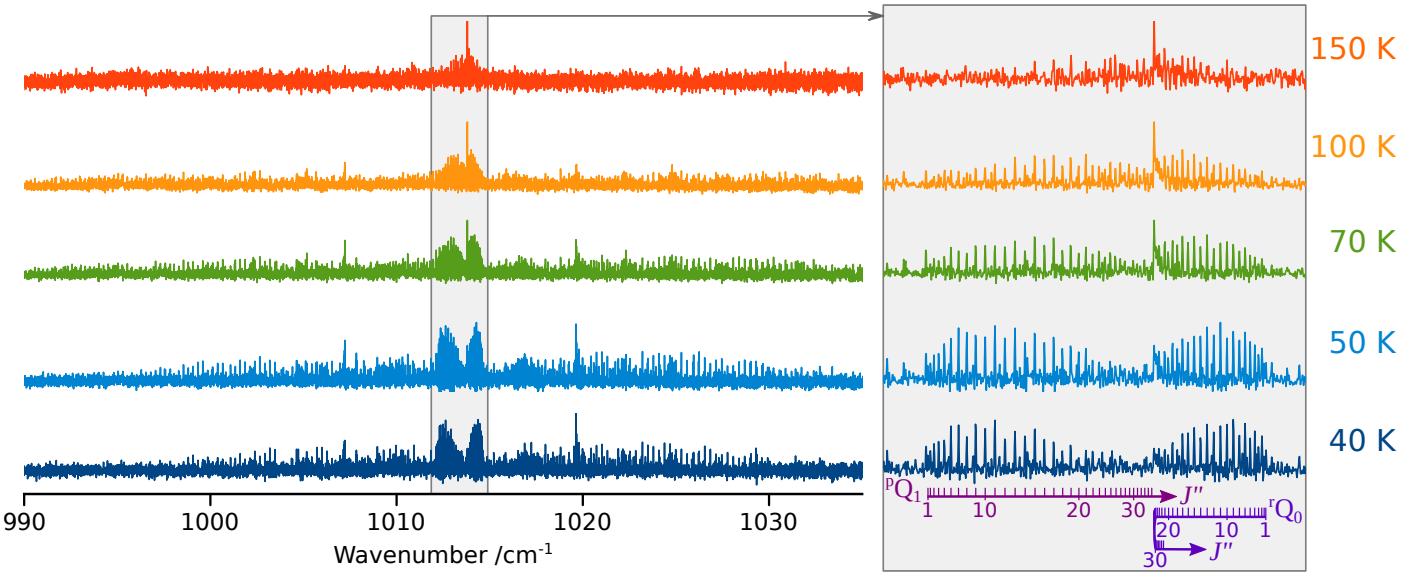


Fig. 6. Evolution of ν_{10} band profile as a function of rotational temperature showing an expanded view of the Q-branch (gray insert). Spectra were all recorded at medium resolution (0.01 cm^{-1}) but with different sample:He ratios. Rotational temperatures determined from simulations of the ν_{11} band profile are indicated on the far right (see text in the Methods section and Fig. S2 for further details).

all assigned transitions to their experimental accuracy (resulting in a reduced standard deviation of 1.1). Taken together with the larger value of D_K in $v_{24} = 1$ compared to that in $v = 0$, this behavior likely indicates $v_{24} = 1$ is somewhat less "rigid" than the ground state.

The situation for the ν_{10} band is significantly more complicated; the band shows obvious signs of a (strong) perturbation. To reproduce as many transitions from the cold spectrum as possible, three sextic (H_K, H_{JK}, and H_{KJ}) CD terms are required. These parameters, however, as well as the quartic CD terms, have magnitudes that are much larger than expected (e.g., D_{JK} is 38 times larger than the ground state value and H_K is 50 times larger than the corresponding value in $v_{24} = 1$). Despite their inclusion, 163 transitions (120 different frequencies) were still rejected from the fit using a 5σ criterion. These transitions are almost exclusively high J values in each K_a branch, meaning that the highest values of J included in the fit decrease with K_a. For completeness these transitions are reported in the Supporting Information. In light of the difficulties encountered in the cold Jet-AILES spectrum, which samples a limited range of rotational excitation, no attempt was made to fit the warm CLS spectrum. Based on the available data it appears that a strong perturbation occurs for $K'_a \geq 4$, likely from the nearly degenerate dark state $\nu_9 + \nu_{12}$, if the VPT2 calculations can be trusted.

Treatment of the perturbation in ν_{10} has been attempted. From our quantum chemical calculations, the $v_9 = v_{12} = 1$ level is predicted to lie at 1034 cm^{-1}, and the interaction between this state and $v_{10} = 1$ is predicted to be Fermi and/or c-type Coriolis, the former with a coupling value of order 0.8 cm^{-1}. The same calculation also predicts $v_{10} = 1$ at 1012.2 cm^{-1} (about 1 cm^{-1} away from the experimental value) and scaled rotational constants that are consistently very close to the experimental values for the other bands investigated in this work, i.e. about 0.2 % for B and C, and 5% for the A constant (see Tables 1 and S2). Nevertheless, no satisfactory fit was obtained for the combined fit, regardless of the magnitude of the coupling parameter. At present, we believe this fitting failure is no accident, but rather due to a coincidence between $K_a = 4$ of $v_{10} = 1$ and the first K_a values in $v_9 = v_{12} = 1$, based on effective Hamiltonian predictions (Fig. 7). This is consistent with the large residuals associated with the $K'_a = 4$ value in the ν_{10} band. The main obstacle is the lack of accurate data on the dark $v_9 = v_{12} = 1$ state: no pure rotational data are available and there is no evidence of the $\nu_9 + \nu_{12}$ band in the experimental spectra, presumably because its calculated intensity is more than two orders of magnitude lower than that of ν_{10}.

While unsatisfactory in some respects, the effective fit reported here improves our understanding of the rovibrational structure of *trans*-butadiene. Concerning the band centers, for instance, the value determined in this work for the ν_{24} band is 2 cm^{-1} lower than the previous value, derived from low-resolution spectroscopy reported in Ref. 15. A much closer agreement is obtained for the ν_{10} band (0.5 cm^{-1}) as a consequence of this band being a c-type, which is characterized by a sharp Q-branch at room temperature. The rotational constants in the ground state are also extremely reliable, since they have now been derived from measurements of roughly 10,000 lines.

Table 1. Rotational constants of butadiene in the ground state, $v_{24} = 1$, and $v_{10} = 1$ after initial assignments using the ASAP software and the final fit in comparison with predicted values. Numbers in parenthesis are one standard deviation in units of the last quoted digit. Brackets indicate parameters fixed to the ground state values.

	$v = 0$	$v_{24} = 1$			$v_{10} = 1$		
Constant	Final	Pred.[a]	Ini. (ASAP)	Final	Pred.[a]	Ini. (ASAP)	Final
E		299.1	297.0970719(258)	297.0923451(62)	1013.8	1013.371993(93)	1013.368967(66)
A	1.39038285(40)	1.3455	1.43140808(57)	1.43163076(55)	1.3950	1.3861088(66)	1.386966(15)
B	0.147885664(59)	0.1478	0.14793757(207)	0.147960763(63)	0.1469	0.14945258(72)	0.14952571(74)
C	0.133694116(62)	0.1338	0.13364383(222)	0.133616011(65)	0.1337	0.13381633(72)	0.13382711(68)
$D_J \times 10^6$	0.0287444(89)	[·]	0.027890(37)	0.0278283(90)	[·]	[·]	0.0470(12)
$D_{JK} \times 10^6$	−0.23874(16)	[·]	−0.22862(60)	−0.24369(17)	[·]	−16.3923(253)	−9.191(57)
$D_K \times 10^6$	7.2929(11)	[·]	19.4396(32)	21.9587(59)	[·]	[·]	53.51(82)
$d_1 \times 10^9$	−3.5988(53)	[·]	[·]	−3.5927(71)	[·]	[·]	[·]
$d_2 \times 10^9$	−0.1883(24)	[·]	[·]	−0.5070(27)	[·]	[·]	[·]
$H_{JK} \times 10^9$							−6.985(70)
$H_{KJ} \times 10^6$							0.3054(15)
$H_K \times 10^9$				8.485(30)			434.(13)
$L_K \times 10^{12}$				−4.010(49)			

	Total	$v_{24} = 1$	ν_{24}	$v_{10} = 1$	ν_{10}
$N(n)$[b]	10663 (9068)	290	2840 (1953)	134	764 (562)
J_{max}, $K_{a\,max}$ [c]	88, 18	44, 14	87, 18	24, 6	26, 7
rms /cm^{-1}	0.00061	0.00085	0.00011	0.00803	0.00075
σ[d]	1.29	8.52	1.08	16.05	1.50

[a] Experimental band centers determined from low-resolution spectroscopy (Ref. 15) and scaled ab initio rotational constants (see text and Tab. S2)
[b] Number of energy levels in ASAP or transitions in SPFIT (N) and number of different frequencies (n) included in the fit (this number may differ from the number of assigned transitions, see text)
[c] Upper state values except in the column "Total" where the ground state values are reported
[d] Reduced standard deviation (unitless)

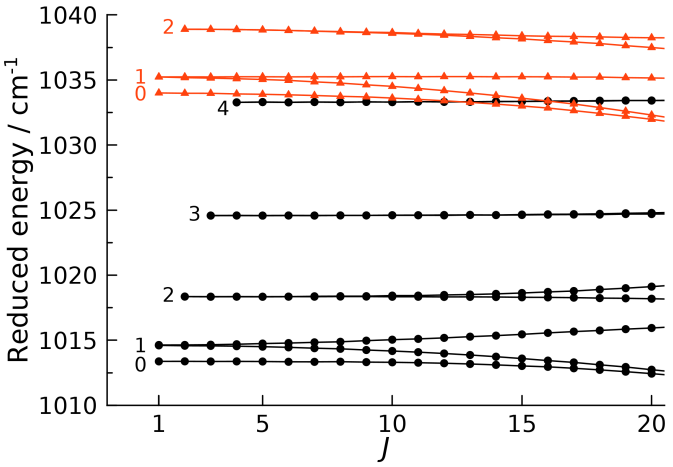


Fig. 7. Rotational energy level diagram in $v_{10} = 1$ (best fit, black dots) and $v_9 = v_{12} = 1$ (best prediction, red triangles). The term $1/2(B+C)J(J+1)$ is subtracted from the energy. K_a values are noted at the head of each series.

4. Conclusions

While attempting to record the ro-vibrational spectrum of *gauche*-butadiene, we have re-investigated the far-infrared spectrum of its more stable *trans* conformer. Two new bands, ν_{24} and ν_{10}, have been observed and assigned, meaning that only one IR active band below 1100 cm^{-1}, namely ν_{23}, has evaded detection at high resolution. The ASAP software was used to initially assign the spectra of both bands in a few hours. While the assignment was straightforward, the fit has proven more challenging since the ν_{10} band appears strongly perturbed, most likely by the dark $v_9 = v_{12} = 1$ state. In absence of any experimental information for this state (rotational constants or band center), no reasonable treatment of the perturbation could be achieved. Further investigation of the species under rotationally cooled conditions may prove useful to determine the $\nu_9 + \nu_{12}$ band centers, and ideally rotational constants, assuming a sufficient signal-to-noise ratio can be reached. Such measurements may also enable the detection of the ν_{23} band. Nevertheless, now that the far-IR ro-vibrational spectrum of the most abundant conformer of butadiene is nearly complete, renewed attempts to assign the *gauche* spectrum can be undertaken with greater confidence.

Supporting Information. Calibration plots (Figure S1); Experimental Jet-AILES spectra and comparison with simulations (Figure S2); Calculated band centers and intensities (Tables S1); Predicted rotational constants (Table S2); Full list of derived rotational constants (Table S3); Literature transitions for which the estimated uncertainty was increased in the present fit (Table S4). Complete list of observed transitions and fit files (in text format).

Acknowledgement

Part of the research described in this paper was performed at the Canadian Light Source, a national research facility of the University of Saskatchewan, which is supported by the Canada Foundation for Innovation (CFI), the Natural Sciences and Engineering Research Council (NSERC), the National Research Council (NRC), the Canadian Institutes of Health Research (CIHR), the Government of Saskatchewan, and the University of Saskatchewan. We acknowledge the SOLEIL facility for provision of synchrotron radiation and we would like to thank the AILES@SOLEIL and Far-IR@CLS beamlines staff for their assistance. This work has been performed under the SOLEIL proposal 20171389 and CLS proposal 27G08965. We thank Mohammed Bali for assistance in the recording of the SOLEIL jet spectrum. MCM and JPP acknowledge support from NASA grant 80NSSC18K0396 and NSF grant CHE-1566266.

References

1. N. C. Craig, P. Groner, and D. C. McKean. Equilibrium Structures for Butadiene and Ethylene: Compelling Evidence for π-Electron Delocalization in Butadiene. *J. Phys. Chem. A*, **110**(23), 7461–7469 (2006). doi:10.1021/jp060695b.
2. K. B. Wiberg, P. R. Rablen, and J. H. Baraban. Butadiene and heterodienes revisited. *J. Org. Chem.*, **83**(15), 8473–8482 (2018). doi:10.1021/acs.joc.8b01085.
3. O. Diels and K. Alder. Synthesen in der hydroaromatischen Reihe. *Justus Liebigs Ann. Chem.*, **460**(1), 98–122 (1928). doi:10.1002/jlac.19284600106.
4. P.-Q. Liao, N.-Y. Huang, W.-X. Zhang, J.-P. Zhang, and X.-M. Chen. Controlling guest conformation for efficient purification of butadiene. *Science*, **356**(6343), 1193–1196 (2017). doi:10.1126/science.aam7232.
5. J. H. Baraban, M.-A. Martin-Drumel, P. B. Changala, S. Eibenberger, M. Nava, D. Patterson, J. F. Stanton, G. B. Ellison, and M. C. McCarthy. The molecular structure of gauche-1,3-butadiene: Experimental establishment of non-planarity. *Angew. Chem. Int. Ed.*, **57**(7), 1821–1825 (2018). doi:10.1002/anie.201709966.
6. V. Schomaker and L. Pauling. The electron diffraction investigation of the structure of benzene, pyridine, pyrazine, butadiene-1,3, cyclopentadiene, furan, pyrrole, and thiophene. *J. Am. Chem. Soc.*, **61**(7), 1769–1780 (1939). doi:10.1021/ja01876a038.
7. K. Kveseth, R. Seip, and D. A. Kohl. Conformational Analysis. The Structure and Torsional Potential of 1,3-Butadiene as Studied by Gas Electron Diffraction. *Acta Chem. Scand.*, **34A**, 31–42 (1980). doi:10.3891/acta.chem.scand.34a-0031.
8. M. Halonen, L. Halonen, and D. J. Nesbitt. Structural issues in conjugated hydrocarbons: High-resolution infrared slit-jet spectroscopy of trans-1,3-butadiene. *J. Phys. Chem. A*, **108**(16), 3367–3372 (2004). doi:10.1021/jp037703y.
9. N. C. Craig, J. L. Davis, K. A. Hanson, M. C. Moore, K. J. Weidenbaum, and M. Lock. Analysis of the rotational structure in bands in the high-resolution infrared spectra of butadiene and butadiene-2,3-d_2: Refinement in assignments of fundamentals. *J. Mol. Struct.*, **695**, 59–69 (2004). doi:10.1016/j.molstruc.2003.11.051.
10. W. Caminati, G. Grassi, and A. Bauder. Microwave Fourier Transform Spectrum of s-trans-1,3-butadiene-1,1-d_2. *Chem. Phys. Lett.*, **148**(1), 13–16 (1988). URL: http://www.sciencedirect.com/science/article/pii/0009261488872518, doi:http://dx.doi.org/10.1016/0009-2614(88)87251-8.
11. N. C. Craig, K. A. Hanson, R. W. Pierce, S. D. Saylor, and R. L. Sams. Rotational analysis of bands in the high-resolution infrared spectra of

the three species of butadiene-1,4-d_2; refinement of the assignments of the vibrational fundamentals. *J. Mol. Spectrosc.*, **228**(2), 401–413 (2004). doi:10.1016/j.jms.2004.07.001.

12. N. C. Craig, K. A. Hanson, M. C. Moore, and R. L. Sams. Rotational analysis of several bands in the high-resolution infrared spectrum of butadiene-1-$^{13}c_1$: Assignment of vibrational fundamentals. *J. Mol. Struct.*, **742**(1-3), 21–29 (2005). doi:10.1016/j.molstruc.2004.11.090.
13. N. C. Craig, M. C. Moore, A. K. Patchen, and R. L. Sams. Analysis of rotational structure in the high-resolution infrared spectrum and assignment of vibrational fundamentals of butadiene-2,3-$^{13}c_2$. *J. Mol. Spectrosc.*, **235**(2), 181–189 (2006). doi:10.1016/j.jms.2005.11.002.
14. N. C. Craig and R. L. Sams. An Investigation of the Rotamers of Butadiene by High-Resolution Infrared Spectroscopy. *J. Phys. Chem. A*, **112**(49), 12637–12646 (2008). URL: http://dx.doi.org/10.1021/jp807677y, doi:10.1021/jp807677y.
15. S. V. Krasnoshchekov, N. C. Craig, P. Boopalachandran, J. Laane, and N. F. Stepanov. Anharmonic Vibrational Analysis of the Infrared and Raman Gas-Phase Spectra of s-trans- and s-gauche-1,3-Butadiene. *J. Phys. Chem. A*, **119**(43), 10706–10723 (2015). doi:10.1021/acs.jpca.5b07650.
16. Y. N. Panchenko, J. V. Auwera, Y. Moussaoui, and G. R. De Mare. Predictive abilities of scaled quantum mechanical molecular force fields: Application to 1,3-butadiene. *Struct. Chem.*, **14**(4), 337–348 (2003). doi:10.1023/A:1024445810013.
17. I. M. Mills. Vibration-Rotation Structure in Asymmetric- and Symmetric-Top Molecules. In K. N. Rao and C. W. Mathews, editors, *Molecular Spectroscopy: Modern Research*. Academic Press, New York (1972).
18. J. Almlöf and P. R. Taylor. General Contraction of Gaussian Basis Sets. I. Atomic Natural Orbitals for First- and Second-row Atoms. *J. Chem. Phys.*, **86**(7), 4070 (1987).
19. J. F. Stanton, J. Gauss, L. Cheng, M. E. Harding, D. A. Matthews, and P. G. Szalay. CFOUR, Coupled-Cluster techniques for Computational Chemistry, a quantum-chemical program package. With contributions from A.A. Auer, R.J. Bartlett, U. Benedikt, C. Berger, et al. For the current version, see http://www.cfour.de.
20. E. Goldstein, B. Beno, and K. Houk. Density functional theory prediction of the relative energies and isotope effects for the concerted and stepwise mechanisms of the diels-alder reaction of butadiene and ethylene. *J. Am. Chem. Soc.*, **118**(25), 6036–6043 (1996).
21. A. McKellar, D. Tokaryk, L.-H. Xu, D. Appadoo, and T. May. High resolution analysis of the ν_{12} and ν_{17} fundamental bands of acrolein, ch_2chcho, in the 600 cm^{-1} region. *J. Mol. Spectrosc.*, **242**(1), 31–38 (2007). doi:10.1016/j.jms.2007.01.005.
22. A. McKellar and D. Appadoo. High-resolution synchrotron far-infrared spectroscopy of acrolein: The vibrational levels below 700 cm^{-1}. *J. Mol. Spectrosc.*, **250**(2), 106–113 (2008). doi:10.1016/j.jms.2008.05.003.
23. I. Gordon, L. Rothman, C. Hill, R. Kochanov, Y. Tan, P. Bernath, M. Birk, V. Boudon, A. Campargue, K. Chance, B. Drouin, J.-M. Flaud, R. Gamache, J. Hodges, D. Jacquemart, V. Perevalov, A. Perrin, K. Shine, M.-A. Smith, J. Tennyson, G. Toon, H. Tran, V. Tyuterev, A. Barbe, A. Császár, V. Devi, T. Furtenbacher, J. Harrison, J.-M. Hartmann, A. Jolly, T. Johnson, T. Karman, I. Kleiner, A. Kyuberis, J. Loos, O. Lyulin, S. Massie, S. Mikhailenko, N. Moazzen-Ahmadi, H. Mueller, O. Naumenko, A. Nikitin, O. Polyansky, M. Rey, M. Rotger, S. Sharpe, K. Sung, E. Starikova, S. Tashkun, J. V. Auwera, G. Wagner, J. Wilzewski, P. Wcisło, S. Yu, and E. Zak. The hitran2016 molecular spectroscopic database. *J. Quant. Spectrosc. Radiat. Transfer*, **203**, 3–69 (2017). HITRAN2016 Special Issue. doi:https://doi.org/10.1016/j.jqsrt.2017.06.038.
24. A. Maki, G. Mellau, S. Klee, M. Winnewisser, and W. Quapp. High-temperature infrared measurements in the region of the bending fundamental of $h^{12}c^{14}n$, $h^{12}c^{15}n$, and $h^{13}c^{14}n$. *J. Mol. Spectrosc.*, **202**(1), 67–82 (2000). doi:10.1006/jmsp.2000.8113.
25. E. Zak, J. Tennyson, O. L. Polyansky, L. Lodi, N. F. Zobov, S. A. Tashkun, and V. I. Perevalov. A room temperature co_2 line list with ab initio computed intensities. *J. Quant. Spectrosc. Radiat. Transfer*, **177**, 31–42 (2016). doi:10.1016/j.jqsrt.2015.12.022.
26. V.-M. Horneman. High accurate peak positions for calibration purposes with the lowest fundamental bands ν_2 of N_2O and CO_2. *J. Mol. Spectrosc.*, **241**(1), 45–50 (2007). doi:10.1016/j.jms.2006.10.014.
27. J.-B. Brubach, L. Manceron, M. Rouzières, O. Pirali, D. Balcon, F. Kwabia-Tchana, V. Boudon, M. Tudorie, T. R. Huet, A. Cuisset, and P. Roy. Performance of the ailes thz-infrared beamline on soleil for high resolution spectroscopy. *AIP Conference Proceedings*, **1214**, 81–84 (2010). doi:10.1063/1.3326356.
28. O. Pirali, V. Boudon, J. Oomens, and M. Vervloet. Rotationally resolved infrared spectroscopy of adamantane. *J. Chem. Phys.*, **136**(2), 024310 (2012). doi:10.1063/1.3666853.
29. F. Matsushima, H. Odashima, T. Iwasaki, S. Tsunekawa, and K. Takagi. Frequency-measurement of pure rotational transitions of H_2O from 0.5 to 5 THz. *J. Mol. Struct.*, **352**, 371–378 (1995).
30. V. M. Horneman, R. Anttila, S. Alanko, and J. Pietilä. Transferring Calibration from CO_2 Laser Lines to Far Infrared Water Lines with the Aid of the ν_2 Band of OCS and the ν_2, ν_1–ν_2, and $\nu_1 + \nu_2$ Bands of $^{13}CS_2$: Molecular Constants of $^{13}CS_2$. *J. Mol. Spectrosc.*, **234**(2), 238–254 (2005). doi:10.1016/j.jms.2005.09.011.
31. M. Cirtog, P. Asselin, P. Soulard, B. Tremblay, B. Madebene, and M. E. Alikhani. The $(CH_2)_2O{-}H_2O$ hydrogen bonded complex. ab initio calculations and fourier transform infrared spectroscopy from neon matrix and a new supersonic jet experiment coupled to the infrared ailes beamline of synchrotron soleil. *J. Phys. Chem. A*, **115**(12), 2523–2532 (2011). doi:{10.1021/jp111507z}.
32. P. Asselin, B. Madebene, P. Soulard, R. Georges, M. Goubet, T. R. Huet, O. Pirali, and A. Zehnacker-Rentien. Competition between inter- and intra-molecular hydrogen bonding: An infrared spectroscopic study of jet-cooled amino-ethanol and its dimer. *J. Chem. Phys.*, **145**(22) (2016). doi:{10.1063/1.4972016}.
33. C. M. Western. PGOPHER: A Program for Simulating Rotational, Vibrational and Electronic Spectra. *J. Quant. Spectrosc. Radiat. Transfer*, **186**, 221–242 (2017). doi:10.1016/j.jqsrt.2016.04.010.
34. M.-A. Martin-Drumel, C. P. Endres, O. Zingsheim, T. Salomon, J. van Wijngaarden, O. Pirali, S. Gruet, F. Lewen, S. Schlemmer, M. C. McCarthy, and S. Thorwirth. The soleil view on sulfur rich oxides: The s_2o bending mode ν_2 at 380 cm^{-1} and its analysis using an automated spectral assignment procedure (asap). *J. Mol. Spectrosc.*, **315**, 72–79 (2015). doi:10.1016/j.jms.2015.02.014.
35. S. Thorwirth, M.-A. Martin-Drumel, C. P. Endres, T. Salomon, O. Zingsheim, J. van Wijngaarden, O. Pirali, S. Gruet, F. Lewen, S. Schlemmer, and M. C. McCarthy. An asap treatment of vibrationally excited s_2o: The ν_3 mode and the $\nu_3 + \nu_2 - \nu_2$ hot band. *J. Mol. Spectrosc.*, **319**, 47–49 (2016). doi:10.1016/j.jms.2015.12.009.
36. Z. Kisiel, L. Pszczółkowski, I. R. Medvedev, M. Winnewisser, F. C. D. Lucia, and E. Herbst. Rotational spectrum of trans-trans diethyl ether in the ground and three excited vibrational states. *J. Mol. Spectrosc.*, **233**(2), 231–243 (2005).
37. W. Lodyga, M. Kreglewski, P. Pracna, and S. Urban. Advanced graphical software for assignments of transitions in rovibrational spectra. *J. Mol. Spectrosc.*, **243**, 182–188 (2007).
38. H. M. Pickett. The fitting and prediction of vibration-rotation spectra with spin interactions. *J. Mol. Spectrosc.*, **148**, 371–377 (1991).